3D ROTATION ESTIMATION USING DISCRETE SPHERICAL HARMONIC OSCILLATOR TRANSFORMS

Soo-Chang Pei[1] *and Chun-Lin Liu*[2]

National Taiwan University[1]; California Institute of Technology[2]
Department of Electrical Engineering[1,2]
No. 1, Sec. 4 Roosevolt Rd. Taipei, Taiwan[1]; 1200 E. California Blvd.,Pasadena, CA 91125, USA[2]
E-mail: pei@cc.ee.ntu.edu.tw[1] and cl.liu@caltech.edu[2]

ABSTRACT

This paper presents an approach to 3D rotation estimation using discrete spherical harmonic oscillator transforms (discrete SHOTs). Discrete SHOTs not only have simple and fast implementation methods but also are compatible with the existing angle estimation algorithms related to spherical harmonics. Discrete SHOTs of the rotated signal follow the same formulation to the Wigner-D matrix as spherical harmonics transforms. Thus, the spherical harmonics related algorithms could be utilized to discrete SHOTs without modification. Furthermore, compared to some existing methods, our approach with discrete SHOTs exhibits higher accuracy, higher precision and improved robustness to noise if the input signal is sampled uniformly on Cartesian grids. The phenomenon results from no interpolations in discrete SHOTs.

Index Terms— Discrete spherical harmonic oscillator transforms, spherical harmonic transforms, rotation estimation, Euler angles, volume data.

1. INTRODUCTION

The 3D rotation angle estimation problem deals with two 3D objects that own identical shapes but are aligned to different directions. Given the samples of both objects, the 3D rotation angles between these objects are estimated. This issue plays a prominent role in pattern recognition [1], computer vision [2], robotics [3], and computerized tomography imaging [4] when the orientation is of interest.

Spherical harmonic transforms (SHTs) offer an approach to the presented issue [1]. It is known that 3D rotation operations are related to the *Wigner-D matrices* in the spherical harmonic domain. The angle estimation problems are converted to estimating the parameters of the Wigner-D matrices when the SHTs are given.

Discrete spherical harmonic oscillator transforms (discrete SHOTs) provide an efficient method to analyzing the spherical components from the Cartesian samples without interpolation [5]. Discrete SHOTs find useful applications in signal expansion, rotational invariance analysis, and MRI data compression. Spherical harmonics in the transform kernels make discrete SHOTs compatible with the algorithms stemming from the SHT. Based on such merit, this paper aims to combine discrete SHOTs with the angle estimation algorithm and to compare the performances of the estimators based on spherical-harmonic-related transforms.

This paper is organized as follows. Section 2 surveys the related work and Section 3 briefly reviews the concept of 3D rotations and Wigner-D matrices. Discrete SHOTs are introduced in Section 4. It is proved in Section 5 that discrete SHOTs are compatible with the existing angle estimation algorithm and the overall system diagram is summarized in Fig. 2. Section 6 experiments on the estimation accuracy and the noise robustness of the proposed method, compared to some existing approaches. Section 7 concludes this paper.

2. RELATION TO PRIOR WORK

Our work considers the angle estimation problem when the input objects are sampled uniformly on the 3D Cartesian coordinates. That is, the input samples are defined on the $\mathbb{R}^3$ grid, also called the *volume* data, used widely in medical imaging. Most angle estimation algorithms with the spherical harmonics work on the *surface* input data [1, 6, 7], where the data is parametrized in terms of the polar angle θ and the azimuthal angle φ. The surface information describes the general outline of the object in 2D but the full energy distribution of the object in 3D is not included.

The angle estimation algorithm proposed by Burel and Hénocq [8] dealt with the angle estimation formulae for spherical harmonics. SHTs were computed over (θ, φ) so that the input signals should be first interpolated to spherical samples and spherical harmonics can only be evaluated on a fixed radius.

Spherical Fourier transforms (SFTs) for rotational invariant features were proposed by Wang et al. [9]. SFTs were defined by a 3D transform kernel with spherical harmonics in its θ- and φ-components. It was proved that SFTs are related to the Wigner-D matrices for rotated objects and the performance would be better than that of the spherical harmonics on a provided radius. However, this work only addressed the rotational invariance rather than rotation angles between objects. In addition, SFTs are also transforms on the spherical coordinates so Cartesian input samples are first converted to spherical samples before applying SFTs.

Presented with the above issues, the angle estimation problem is reconsidered in this paper. For Cartesian samples, we utilized discrete SHOTs to perform this task. Discrete SHOTs analyze the spherical components of volume data without any coordinate conversion. Besides, it will be proved that the angle estimation algorithms proposed in [8] are compatible with discrete SHOTs, inspired by [9]. Hence, higher accuracy could be expected when discrete SHOTs and the angle estimation formulae [8] are cascaded.

3. PRELIMINARY

3.1. The rotation operation in three-dimensions

A 3D position vector $\mathbf{r}$ can be specified on the Cartesian coordinate system $(x, y, z) \in \mathbb{R}^3$ or on the spherical coordinate system, char-

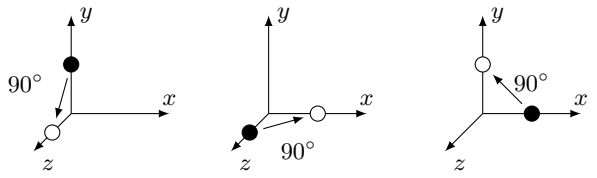

(a) X-rotation (b) Y-rotation (c) Z-rotation

Fig. 1. The rotation operation around (a) x-axis, (b) y-axis and (c) z-axis by 90°, respectively. The solid circles indicate the original objects while the empty circles show the new objects after rotation.

acterized by the distance to the origin r, the polar angle θ, and the azimuthal angle φ. These parameters are defined over $r \in [0, \infty)$, $\theta \in [0, \pi]$, and $\varphi \in [0, 2\pi)$. The coordinates are uniquely related by $x = r \sin\theta \cos\varphi$, $y = r \sin\theta \sin\varphi$ and $z = r \cos\theta$.

The 3D rotation is specified by Euler angles [10]. Any 3D rotation can be decomposed into the three basic rotation operations with respect to certain axes, as illustrated in Fig. 1. The Euler angles cascade the basic rotations and parametrize the corresponding rotation angles. In this paper, the ZYZ convention for Euler angles is adapted. That is, the object is first rotated by α around z-axis, then followed by a rotation β around the y-axis in the rotated coordinate, and finally rotated by γ around the resultant z-axis, where $\alpha, \gamma \in [0, 2\pi]$ and $\beta \in [0, \pi]$. The three Euler angles are described by the operator $\mathcal{R}_{\alpha,\beta,\gamma}$, where the three rotation angles are specified in order.

The Euler angles uniquely determine the 3D rotation except $\beta = 0, \pi$. If $\beta = 0$, the rotation is equivalent to successive Z-rotations by α and γ so that $\alpha + \gamma$ is unique rather than α and γ. On the other hand, $\beta = \pi$ results in unique $\alpha - \gamma$.

3.2. Spherical harmonic transforms and Wigner-D matrices

Spherical harmonics are defined over (θ, φ) as

$$Y_{\ell m}(\theta, \varphi) = (-1)^m \sqrt{\frac{2\ell+1}{4\pi} \frac{(\ell-m)!}{(\ell+m)!}}\, P_\ell^m(\cos\theta)\, e^{jm\varphi}, \quad (1)$$

where $\ell = 0, 1, 2, \ldots, -\ell \le m \le \ell$ and $P_\ell^m(\cdot)$ denote the associated Legendre polynomials. Considering a surface signal $f(\theta, \varphi)$, its spherical harmonic transforms (SHTs) $F_{\ell,m}$ are the inner products between $f(\theta, \varphi)$ and $Y_{\ell m}(\theta, \varphi)$ over the angles [8],

$$F_{\ell,m} = \int_0^{2\pi} \int_0^{\pi} f(\theta, \varphi) Y_{\ell m}^*(\theta, \varphi) \sin\theta \mathrm{d}\theta \mathrm{d}\varphi. \quad (2)$$

For the Euler rotation α, β, γ on $f(\theta, \varphi)$, the SHTs after rotation ($F_{\ell,m}(\alpha, \beta, \gamma)$) are related to the SHTs before rotation ($F_{\ell,m'}$) by

$$F_{\ell,m}(\alpha, \beta, \gamma) = \sum_{m'=-\ell}^{\ell} D_{m,m'}^{\ell}(\alpha, \beta, \gamma) F_{\ell,m'}, \quad (3)$$

where $-\ell \le m, m' \le \ell$ and $D_{m,m'}^{\ell}(\alpha, \beta, \gamma)$ are the elements of the Wigner-D matrix. (3) can be rewritten as matrix operation when $\{F_{\ell,m}\}_{m=-\ell,\ldots,\ell}$ are modeled as a vector and $D_{m,m'}^{\ell}(\alpha, \beta, \gamma)$ establish squared matrices of size $2\ell+1$, called the Wigner-D matrices. Values and properties of the Wigner-D matrices are referred to [8].

4. DISCRETE SPHERICAL HARMONIC OSCILLATOR TRANSFORMS

Spherical harmonic oscillator wavefunctions (SHOWs) originated from the wavefunctions of quantum harmonic oscillator systems in spherical coordinates [11]. Based on the system model, Schrödinger's equation for this system is written as

$$\frac{1}{2}\left(r^2 - \nabla^2\right) \langle \mathbf{r} | n\ell m \rangle = \left(N + \frac{3}{2}\right) \langle \mathbf{r} | n\ell m \rangle, \quad (4)$$

where ∇^2 denotes the 3D Laplacian operator and $N = 2n + \ell$ is the *order* of the SHOWs. The bracket notations of SHOWs are denoted by $\langle \mathbf{r} | n\ell m \rangle$, indexing by integer parameters n, ℓ, and m, where $n, \ell = 0, 1, 2, \ldots; m = -\ell, -\ell+1, \ldots, \ell-1, \ell$. The physical meaning of the bracket notation can be referred to [5, 10, 11] for the interested readers. (4) is solved to be [11]

$$\langle \mathbf{r} | n\ell m \rangle = N_{n\ell} r^\ell L_n^{\ell+1/2}\left(r^2\right) e^{-r^2/2} Y_{\ell m}(\theta, \varphi), \quad (5)$$

where $N_{n\ell}$ is the normalization factor related to n, ℓ and $L_n^\alpha(\cdot)$ are the associated Laguerre polynomials. SHOWs were proved to form a complete and orthonormal basis for $L^2\left(\mathbb{R}^3\right)$, the set of finite-energy signals in 3D [11].

Alternatively, the wavefunctions for the quantum harmonic oscillator can also be solved on the Cartesian coordinates, i.e. solving (4) for $\mathbf{r} = (x, y, z)$, yielding separable Hermite Gaussian functions as the wavefunctions,

$$\langle \mathbf{r} | n_x n_y n_z \rangle = K e^{-\frac{x^2+y^2+z^2}{2}} H_{n_x}(x) H_{n_y}(y) H_{n_z}(z), \quad (6)$$

where K denotes the normalization factor, $H_n(\cdot)$ are the Hermite polynomials and the indices $n_x, n_y, n_z = 0, 1, 2, \ldots$. The *order* of the separable Hermite Gaussian function is $N = n_x + n_y + n_z$. It is obvious that (6) is separable in the Cartesian coordinates. Separable Hermite Gaussian functions are also complete and orthonormal basis for $L^2\left(\mathbb{R}^3\right)$.

In [12, 13], SHOWs and separable Hermite Gaussian functions are related to each other by the transformation coefficients $C_{n_x,n_y,n_z}^{n,\ell,m}$

$$\langle \mathbf{r} | n\ell m \rangle = \sum C_{n_x,n_y,n_z}^{n,\ell,m} \langle \mathbf{r} | n_x n_y n_z \rangle, \quad (7)$$

where the summation runs over all n_x, n_y, n_z with $n_x + n_y + n_z = 2n + \ell = N$. (7) implies *the SHOWs of order N are the finite linear combination of the separable Hermite Gaussian functions of order N*. Once $C_{n_x,n_y,n_z}^{n,\ell,m}$ is computed, the SHOWs, which are spherically symmetric, can be synthesized from the separable Hermite Gaussian functions, which are separable in the Cartesian coordinates. In addition, the summation in (7) is finite, indicating that (7) can be evaluated without any truncation error. The closed-form expression for $C_{n_x,n_y,n_z}^{n,\ell,m}$ was studied in [12,13] while a fast computation algorithm for $C_{n_x,n_y,n_z}^{n,\ell,m}$ was proposed in [5].

Spherical harmonic oscillator transforms (SHOTs) are the inner products between SHOWs and the 3D input signal $f(\mathbf{r})$ [5, 11],

$$(n\ell m | f\rangle = \iiint f(\mathbf{r}) \langle \mathbf{r} | n\ell m \rangle^* \, \mathrm{d}^3\mathbf{r}, \quad (8)$$

where $\mathrm{d}^3\mathbf{r} = r^2 \sin\theta \mathrm{d}r\mathrm{d}\theta\mathrm{d}\varphi$ denotes the measure on the spherical coordinates. Separable Hermite transforms, $\langle n_x n_y n_z | f\rangle$, are obtained from the inner products between $f(\mathbf{r})$ and separable Hermite Gaussian functions $\langle \mathbf{r} | n_x n_y n_z \rangle$ [14],

$$\langle n_x n_y n_z | f\rangle = \iiint f(\mathbf{r}) \langle \mathbf{r} | n_x n_y n_z \rangle^* \, \mathrm{d}^3\mathbf{r}, \quad (9)$$

where the measure in (9) is $\mathrm{d}^3\mathbf{r} = \mathrm{d}x\mathrm{d}y\mathrm{d}z$.

In [5], SHOTs and separable Hermite transforms can be related as the finite linear combination of the transform coefficients as

$$(n\ell m|f\rangle = \sum \left(C^{n,\ell,m}_{n_x,n_y,n_z}\right)^* \langle n_x n_y n_z|f\rangle, \tag{10}$$

for all $n_x + n_y + n_z = 2n + \ell = N$. (10) provides an approach to discrete SHOTs:

- Discrete SHOTs can be directly computed on the *Cartesian coordinates*. Although SHOTs are originally defined on the spherical coordinates (8), it is unnecessary to convert the Cartesian samples to the spherical samples, which would introduce additional interpolation error. Instead, if the the input signal $f(\mathbf{r})$ is sampled on the Cartesian grids, the separable Hermite transform can be applied first and then adjust the Hermite transform coefficients with respect to $C^{n,\ell,m}_{n_x,n_y,n_z}$ by (10).
- The algorithm is *fast*. To implement discrete SHOTs, fast algorithms for Hermite transform [15] can be utilized separately in different dimensions. A fast algorithm for the transformation coefficients $C^{n,\ell,m}_{n_x,n_y,n_z}$ was proposed in [5] using the fast Fourier transform algorithm. Furthermore, $C^{n,\ell,m}_{n_x,n_y,n_z}$ are independent of $f(\mathbf{r})$ so that they could be pre-computed and accelerated by table look-up.

5. ROTATION ANGLE ESTIMATION USING DISCRETE SPHERICAL HARMONIC OSCILLATOR TRANSFORMS

In this section, it will be shown that discrete SHOTs can be applied to the angle estimation problem without modifications and the overall system diagram is illustrated in Fig. 2.

To begin with, discrete SHOTs are proved to follow similar relationships with the Wigner-D matrix (3), which is inspired by [9, 16]

Theorem 1. *Consider a finite energy signal $f(\mathbf{r}) \in L^2(\mathbb{R}^3)$ and its SHOTs, $(n\ell m|f\rangle$. Assume that $(n\ell m|f\rangle(\alpha,\beta,\gamma)$ represent the SHOTs of $f(\mathcal{R}_{\alpha,\beta,\gamma}\mathbf{r})$, where $\mathcal{R}_{\alpha,\beta,\gamma}$ denotes the Euler rotation with angles α, β, and γ. Then*

$$(n\ell m|f\rangle(\alpha,\beta,\gamma) = \sum_{m'=-\ell}^{\ell} D^{\ell}_{m,m'}(\alpha,\beta,\gamma)\left(n\ell m'|f\right\rangle, \tag{11}$$

where $D^{\ell}_{m,m'}(\alpha,\beta,\gamma)$ denote the entries of the Wigner-D matrices, as specified in (3).

Proof. Starting from the left-hand side of (11),

$$(n\ell m|f\rangle(\alpha,\beta,\gamma) = \iiint f(\mathcal{R}_{\alpha,\beta,\gamma}\mathbf{r})\langle\mathbf{r}|n\ell m)^* \,\mathrm{d}^3\mathbf{r}. \tag{12}$$

Letting $\mathbf{r}' = \mathcal{R}_{\alpha,\beta,\gamma}\mathbf{r} = (r',\theta',\varphi')$ yields the measure $\mathrm{d}^3\mathbf{r} = \mathrm{d}^3\mathbf{r}'$ and the SHOWs $\langle\mathbf{r}|n\ell m) = \left\langle\mathcal{R}^{-1}_{\alpha,\beta,\gamma}\mathbf{r}'|n\ell m\right\rangle$ becomes

$$N_{n\ell} r^{\ell} L_m^{\ell+1/2}\left(r^2\right) e^{-r^2/2} Y_{\ell m}\left(\mathcal{R}^{-1}_{\alpha,\beta,\gamma}(\theta',\varphi')\right). \tag{13}$$

(13) results from the radius component is invariant under the rotation operation, i.e. $r' = r$. Then, according to the relationships between the spherical harmonics and the Wigner-D matrices, $Y_{\ell m}\left(\mathcal{R}^{-1}_{\alpha,\beta,\gamma}(\theta',\varphi')\right) = \sum\left(D^{\ell}_{m,m'}\right)^* Y_{\ell m}(\theta',\varphi')$ [10], we obtain

$$\langle\mathcal{R}^{-1}_{\alpha,\beta,\gamma}\mathbf{r}'|n\ell m) = \sum_{m=-l}^{l}\left(D^{\ell}_{m,m'}\right)^*\langle\mathbf{r}'|n\ell m). \tag{14}$$

Combining (12) and (14) proves the Theorem 1. □

The similar proof can be found in the appendix of [16] but the definition of spherical harmonics in [9, 16] is slightly different from that in this paper. Theorem 1 resembles (3) except an additional parameter n. For a fixed $n = n_0$, the SHOTs $(n_0\ell m|f\rangle$ are related to $(n_0\ell m|f\rangle(\alpha,\beta,\gamma)$ with Wigner-D matrices exactly. Hence, the algorithms involving SHTs can be directly utilized to SHOTs for a given n_0.

The angle estimation algorithm we adopt here is the one in [8]. Here we choose the estimation formulae from the set $\mathcal{E}_1$. For the input signal $f(\mathbf{r})$, the Euler angles with respect to the *reference signal* are

$$\hat{\alpha}_f = \measuredangle\left(n_0 11|f\rangle\right), \tag{15}$$

$$\hat{\beta}_f = \arctan\left(-\frac{\sqrt{2}\,(n_0 11|f\rangle\,(\hat{\alpha}_f,0,0)}{(n_0 10|f\rangle\,(\hat{\alpha}_f,0,0)}\right), \tag{16}$$

$$\hat{\gamma}_f = \measuredangle\left(n_0 21|f\rangle\left(\hat{\alpha}_f,\hat{\beta}_f,0\right)\right), \tag{17}$$

where the subscript f means these angles are estimated from $f(\mathbf{r})$, $\measuredangle$ denotes the angle of a complex number and the SHOTs with the angles follow the definition in (11). (15) - (17) can be also performed separately on another signal $g(\mathbf{r})$, leading to the estimates $\hat{\alpha}_g$, $\hat{\beta}_g$, and $\hat{\gamma}_g$, as illustrated in Fig. 2.

The Euler angles between $f(\mathbf{r})$ and $g(\mathbf{r})$ then will be combined together from the estimates in the previous step. Based on the Euler angles, we can construct the 3-by-3 rotation matrix directly, denoted by $\mathbf{R}_{\hat{\alpha}_f,\hat{\beta}_f,\hat{\gamma}_f}$ and $\mathbf{R}_{\hat{\alpha}_g,\hat{\beta}_g,\hat{\gamma}_g}$ for $f(\mathbf{r})$ and $g(\mathbf{r})$, respectively. The overall rotation matrix is

$$\mathbf{R}_{\hat{\alpha},\hat{\beta},\hat{\gamma}} = \mathbf{R}^{-1}_{\hat{\alpha}_g,\hat{\beta}_g,\hat{\gamma}_g}\mathbf{R}_{\hat{\alpha}_f,\hat{\beta}_f,\hat{\gamma}_f}. \tag{18}$$

The final step is to estimate Euler angles $\hat{\alpha}$, $\hat{\beta}$, and $\hat{\gamma}$, directly from the entries of the overall rotation matrix.

Fig. 2 serves as a summary on the angle estimation algorithm using discrete SHOTs. First, the discrete SHOTs of the input signals $f(\mathbf{r})$ and $g(\mathbf{r})$ are computed with separable Hermite transforms and fast combination coefficients. The Euler angles with respect to the references are evaluated to have six angle estimates. Finally, establishing the rotation matrices based on the six estimates yields the overall Euler angles $\hat{\alpha}$, $\hat{\beta}$, $\hat{\gamma}$.

6. EXPERIMENTAL RESULTS

In this section, the performance of the proposed algorithm is evaluated and compared to other schemes based on SHTs [8] and SFTs [9]. To simulate Fig. 2, the input signal $f(\mathbf{r})$ is chosen to be mixtures of three Gaussian functions with gains $1, -0.2, -1$, centers $(0,0,1)$, $(1,1,0)$, $(-0.5,-0.5,-1)$, variances $\sigma_x^2 = 4,1,1$, $\sigma_y^2 = 2,1,1$, $\sigma_z^2 = 1,1,1$, respectively. $f(\mathbf{r})$ is sampled uniformly on Cartesian grids with the number of points $N_{\text{pt}} = 31$ and the sampling interval $\Delta = \sqrt{2\pi/N_{\text{pt}}}$. The other input signal $g(\mathbf{r})$ is generated from the rotated version of $f(\mathbf{r})$, where the Euler angles α,β,γ are randomly drawn from their domains. Having the samples of $f(\mathbf{r})$ and $g(\mathbf{r})$, we apply the proposed algorithm to estimate Euler angles $\hat{\alpha},\hat{\beta},\hat{\gamma}$, compared to the actual Euler angles α,β,γ. We also interchange the discrete SHOT block with bilinear interpolation as well as SHTs/SFTs. The parameter $n_0 = 1$ and the radius evaluating SHTs is 1.

The Monte-Carlo test is repeated 1000 times and the relationships between the ground truth α,β,γ and the estimates $\hat{\alpha},\hat{\beta},\hat{\gamma}$ are shown in Fig. 3, where $\alpha+\gamma$ and β are selected. All methods exhibit

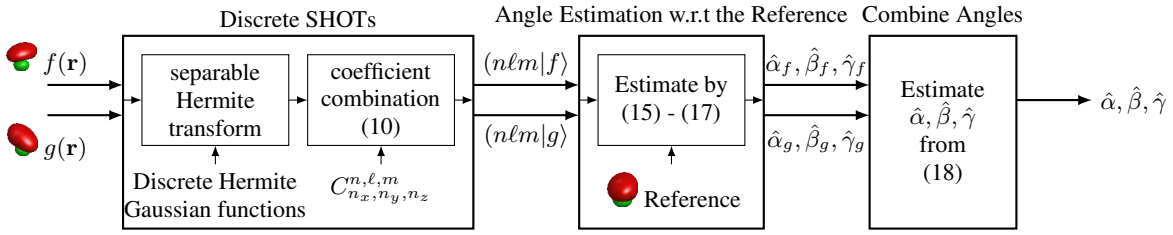

Fig. 2. The overall system diagram of 3D rotation estimation using the discrete SHOTs.

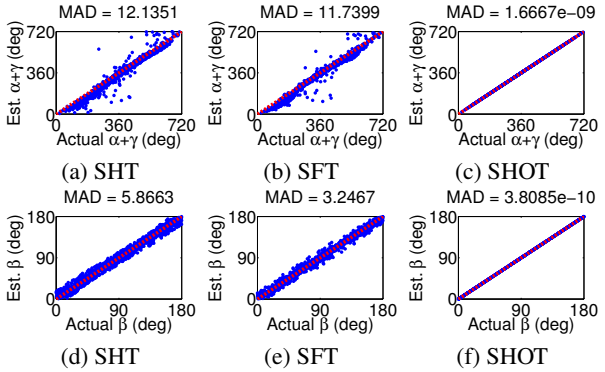

Fig. 3. The scatter plots show the correlations between the estimated Euler angles versus the actual Euler angles when (a), (d) SHTs, (b), (e) SFTs, and (c), (f) SHOTs are utilized. The 1000 blue dots represent different tests of the proposed algorithm. The red dashed line indicates the theoretical curve of the estimators. The median absolute deviations (MADs) in degrees are listed on the top of each plot to show the dispersion of the dots with respect to the theoretical line.

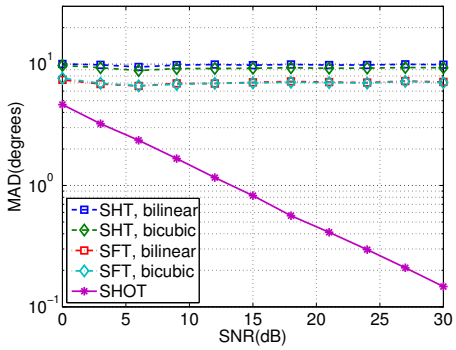

Fig. 4. The noise robustness of the proposed angle estimation algorithm. Each point is obtained from 1000 Monte-Carlo tests of Fig. 2 with random Euler angles and the additive white Gaussian noise. The bilinear/bicubic interpolations are used in SHTs and SFTs.

positive correlation and SHOTs achieve the best fit with the theoretical curve and own the smallest dispersion. To measure the dispersion robustly, the median absolute deviation (MAD)

$$\mathrm{MAD}(x) = \mathrm{median}\left(|x_i - \mathrm{median}(x)|\right), \tag{19}$$

is computed over differences between the actual angles and their estimates. From Fig. 3, these MADs prove our algorithm not only achieves high accuracy but also good precision.

The next experiment simulates the noise robustness in our scenario. We repeated 1000 runs with additive white Gaussian noise and then evaluated MADs with respect to the cascaded sequences of $\hat{\alpha} + \hat{\gamma}$ and $\hat{\beta}$, as listed in Fig. 4. Note that the MADs in Fig. 3 can be considered the noise-free MADs as the lower bounds of the curves in Fig. 4. First of all, the MADs of SHTs and SFTs become saturated for the high-SNR case. The MADs are approximately 10° and 7° for SHTs and SFTs, respectively, and those values are consistent with the MADs without noise, as displayed in Fig. 3(a,b,d,e). Secondly, higher-order interpolation provides limited improvement on the performance. For instance, compared to the bilinear interpolation and the bicubic interpolation, the MADs of SHTs are lowered by only 0.6° while those of SFTs are decreased by 0.1°. However, the SHOT does not suffer from those disadvantages. In Fig. 4, the curve of SHOTs continuously decreases as the SNR increases, rather than the saturation phenomenon of the other two methods. In fact, for the SNR higher than 30dB, the MADs for SHOTs become lower than 0.1° and will reach the level of $\left(10^{-9}\right)^\circ$ eventually, as referred to Fig. 3(c,f).

Fig. 4 indicates that interpolations introduce *interpolation error* to the system. The interpolation error depends on the interpolation methods and dominates the performance when the external noise diminishes. Discrete SHOTs, however, avoid the interpolation error and hence exhibit better performance than the other two methods.

In addition, our simulation considers Cartesian samples of bandlimited signals, which are consistent with Fig. 4(a) in [5]. If non-bandlimited signals or spherical samples are applied to our algorithm, the overall performance would be similar to that of SHTs or SFTs, from the rotational invariance experiment in Fig. 4(b-d) of [5].

The complexity of Fig. 2 is governed by the transforms since angle estimation blocks are independent of N_{pt}. SHTs take $C_1 N_{\mathrm{pt}}^2$ steps for interpolation and approximately $C_2 N_{\mathrm{pt}}^2$ operations for 2D separable transforms, where C_1 depends on interpolation methods and C_2 denotes the number of $F_{\ell,m}$ needed in (15)-(17). The complexity for SFTs is about $(C_1 + C_2) N_{\mathrm{pt}}^3$. Discrete SHOTs require $C_3 N_{\mathrm{pt}}^3$ operations in separable Hermite transforms and a fixed number of operations in transformation coefficients, where C_3 is the number of separable Hermite transforms required in (15)-(17).

7. CONCLUSION

A novel angle estimation algorithm using discrete SHOTs was presented in this paper. We showed that discrete SHOTs not only are compatible with the SHT-based algorithms, but also outperform those utilizing SHTs and SFTs. The advantages of discrete SHOTs result from direct signal analysis on the Cartesian coordinates. Our work could be applied to 3D object alignment, registration, and retrieval for volume data with few modification to the existing framework and might have better performance.

8. REFERENCES

[1] M. Kazhdan, "An Approximate and Efficient Method for Optimal Rotation Alignment of 3D Models," *IEEE Trans. Pattern Anal. Mach. Intell.*, vol. 29, no. 7, pp. 1221–1229, 2007.

[2] D. Saupe and D. Vranić, "3D Model Retrieval with Spherical Harmonics and Moments," in *Pattern Recogn.*, B. Radig and S. Florczyk, Eds., vol. 2191 of *Lecture Notes in Computer Science*, pp. 392–397. Springer Berlin Heidelberg, 2001.

[3] A. Makadia, L. Sorgi, and K. Daniilidis, "Rotation Estimation from Spherical Images," in *Proc. of 2004 ICPR*, 2004, vol. 3, pp. 590–593 Vol.3.

[4] E. Garboczi, "Three-dimensional mathematical analysis of particle shape using X-ray tomography and spherical harmonics: Application to aggregates used in concrete ," *Cement Concrete Res.*, vol. 32, no. 10, pp. 1621–1638, 2002.

[5] S.-C. Pei and C.-L. Liu, "Discrete spherical harmonic oscillator transforms on the Cartesian grids using transformation coefficients," *IEEE Trans. Signal Process.*, vol. 61, no. 5, pp. 1149 – 1164, 2013.

[6] M. Kazhdan, T. Funkhouser, and S. Rusinkiewicz, "Rotation invariant spherical harmonic representation of 3D shape descriptors," in *Proceedings of the 2003 Eurographics/ACM SIGGRAPH symposium on Geometry processing*, Aire-la-Ville, Switzerland, Switzerland, 2003, SGP '03, pp. 156–164, Eurographics Association.

[7] S. Althloothi, M. H. Mahoor, and R. M. Voyles, "A Robust Method for Rotation Estimation Using Spherical Harmonics Representation," *IEEE Trans. Image Process.*, vol. 22, no. 6, pp. 2306–2316, 2013.

[8] G. Burel and H. Hénocq, "Determination of the orientation of 3D objects using spherical harmonics," *Graph. Models Image Process.*, vol. 57, no. 5, pp. 400–408, 1995.

[9] Q. Wang, O. Ronneberger, and H. Burkhardt, "Rotational Invariance Based on Fourier Analysis in Polar and Spherical Coordinates," *IEEE Trans. Pattern Anal. Mach. Intell.*, vol. 31, no. 9, pp. 1715–1722, 2009.

[10] E. P. Wigner, *Group theory and its application ot quantum mechanics of atom spectra*, Academic Press, 1959.

[11] D. J. Griffiths, *Introduction to Quantum Mechanics*, Pearson Prentice Hall, 2 edition, 2004.

[12] K. T. R. Davies and S. J. Krieger, "Harmonic-oscillator transformation coefficients," *Can. J. Phys.*, vol. 69, no. 1, pp. 62–69, 1991.

[13] E. Chacón and M. de Llano, "Transformation brackets between Cartesian and Angular Momentum Harmonic Oscillator Basis Functions with and without Spin-Orbit Coupling Tables for the 2s-1d Nuclear Shell," *Revista Mexicana de Fisica*, vol. XII, no. 2, pp. 5768, 1963.

[14] J.-B. Martens, "The Hermite transform-theory," *IEEE Trans. Acoust., Speech, Signal Process.*, vol. 38, no. 9, pp. 1595–1606, 1990.

[15] G. Leibona, D. N. Rockmorea, W. Parkc, R. Taintora, and G. S. Chirikjianc, "A fast Hermite transform," *Theor. Comput. Sci.*, vol. 409, no. 2, pp. 211228, 2008.

[16] Q. Wang, O. Ronneberger, and H. Burkhardt, "Fourier Analysis in Polar and Spherical Coordinates," 2008.